ORNL/TM-2024/3452

ROADRUNNER MiniFuel Experiment: Irradiation Target Design and Specimen Characterization

A.G. Le Coq
A.M. Schrell
J.L. Salcedo Perez
Z. Karriem
D. Adorno Lopes
G.W. Helmreich
Z.G. Wallen
J.P. Gorton
N.A. Capps
J.M. Harp
K.D. Linton
J.T. White (LANL)
E.S. Sooby (UTSA)

September 2024

OAK RIDGE National Laboratory

ORNL IS MANAGED BY UT-BATTELLE LLC FOR THE US DEPARTMENT OF ENERGY

ORNL/TM-2024/3452

Nuclear Science User Facilities

ROADRUNNER MINIFUEL EXPERIMENT: IRRADIATION TARGET DESIGN AND SAMPLE CHARACTERIZATION

A.G. Le Coq
A.M. Schrell
J.L. Salcedo Perez
Z. Karriem
D. Adorno Lopes
G.W. Helmreich
Z.G. Wallen
J.P. Gorton
N.A. Capps
J.M. Harp
K.D. Linton
J.T. White (LANL)
E.S. Sooby (UTSA)

September 2024

Prepared by
OAK RIDGE NATIONAL LABORATORY
Oak Ridge, TN 37831
managed by
UT-BATTELLE LLC
for the
US DEPARTMENT OF ENERGY
under contract DE-AC05-00OR22725

CONTENTS

LIST OF FIGURES

LIST OF TABLES

ABBREVIATIONS

HFIR	High Flux Isotope Reactor
HGR	heat generation rate
LANL	Los Alamos National Laboratory
MCNP	Monte Carlo N-Particle
NSUF	Nuclear Science User Facilities
ORIGEN	Oak Ridge Isotope Generator
ORNL	Oak Ridge National Laboratory
PIE	post-irradiation examination
RA	radial axial
RB	removable beryllium
ROADRUNNER	Research On ADvancing the peRformance of UraNium Nitrides in Extreme enviRonments
SiC	silicon carbide
TAVA	time-averaged volume-averaged
TD	theoretical density
TM	temperature monitor
UN	uranium nitride
UTSA	University of Texas at San Antonio
XCT	x-ray computed tomography
XRD	x-ray diffraction

ACKNOWLEDGMENTS

This work was performed under the US Department of Energy – Office of Nuclear Energy's Nuclear Science User Facilities (NSUF) program. The co-authors would like to acknowledge Julian Valdez, Anthony Horsman, and Valeria Cantu Vessi at the University of Texas at San Antonio for their work on thinning down the pellets, inspecting, and collecting SEM images of each specimen.

ABSTRACT

High-density uranium nitride (UN) is a fuel candidate for several advanced nuclear reactor designs currently under development. Because there are limited UN performance data relative to fuel fabrication impurity and density variation, an irradiation campaign has been developed as part of a collaborative effort among the University of Texas at San Antonio (UTSA), Westinghouse Electric Company, Oak Ridge National Laboratory (ORNL), and Los Alamos National Laboratory (LANL) under the Nuclear Science User Facilities program. This project, entitled ROADRUNNER, or Research On ADvancing the peRformance of UraNium Nitrides in Extreme enviRonments, aims to support UN fuel qualification for advanced reactors by investigating the impact of density and impurity variations on UN performance as a function of irradiation temperature and burnup. The MiniFuel experiment vehicle developed by ORNL, which leverages the High Flux Isotope Reactor, was selected to perform this accelerated separate-effects irradiation testing. The experiment test matrix consists of six MiniFuel targets containing miniature UN fuel disks, and targets three distinct burnup levels (37.5, 60, and 75 MWd/kg U) and three distinct temperatures (600, 900, and 1200°C). Neutronics and thermal analyses were performed to determine the experimental parameters needed to meet the desired irradiation conditions and to predict the experiment components temperatures. UN pellets were fabricated at LANL with tightly controlled parameters to produce specimens with three distinct densities and three levels of carbon content. The pellets were then thinned down by UTSA to the experiment-required thickness. The pre-characterization of the specimens includes density measurements, carbon and oxygen contents, microstructure analysis, and x-ray computed tomography. The selected specimens will be assembled into the MiniFuel experiment, and the first ROADRUNNER MiniFuel targets are intended for HFIR insertion during the Fall of 2024. After irradiation, the targets will be shipped to ORNL's hot cell facility for disassembly. The post-irradiation examination on the fuel specimens includes fission gas release measurements, visual inspection, fuel swelling measurements, gamma spectroscopy, and microstructure analysis. The data collected post-irradiation will be used to develop fuel performance models.

1. INTRODUCTION

Several advanced nuclear reactor designs under development—such as liquid metal–cooled fast reactors, small modular reactors, microreactors, and surface fission space reactors—are considering high-density uranium nitride (UN) as a fuel candidate to achieve their required performance. Existing data on UN fuel performance were derived primarily from rodlet experiments performed under the space reactor program SNAP [1] and considered burnup and starting density as variables. However, UN performance data relative to the fuel fabrication impurity (carbon and oxygen content), pore nature, and starting microstructure are limited. This lack of data leads to knowledge gaps and sources of high uncertainty in UN fuel performance [2].

To address UN data gaps and to support fuel qualification for advanced reactors, an irradiation campaign entitled *Research On ADvancing the peRformance of UraNium Nitrides in Extreme enviRonments* (ROADRUNNER) has been developed as part of a collaboration among the University of Texas at San Antonio (UTSA), Westinghouse Electric Company, Oak Ridge National Laboratory (ORNL), and Los Alamos National Laboratory (LANL) under the Nuclear Science User Facilities (NSUF) program. The goal of this irradiation campaign is to investigate the impact of bulk and microstructural variations that originate in fuel fabrication on the irradiation performance of UN as a function of both irradiation temperature and burnup. The data collected post-irradiation will be used to develop fuel performance models. UN specimens fabricated at LANL with tightly controlled parameters such as density, impurity, and resulting grain size will be irradiated in ORNL's High Flux Isotope Reactor (HFIR) using the MiniFuel experiment design [3][4][5]. The fuel specimens were characterized at LANL, UTSA, and ORNL. This report summarizes the ROADRUNNER MiniFuel irradiation test matrix, the experiment design, and the fuel specimen characterization.

2. EXPERIMENT TEST MATRIX

The experimental test matrix comprises six MiniFuel targets containing depleted UN disk specimens. These samples will be irradiated in HFIR's removable beryllium (RB) reflector. The irradiation conditions target three distinct discharge burnups (low-, mid-, and high-burnup) and three distinct temperatures. Table 1 summarizes the experiment test matrix. Target RRN01 aims to provide several high-purity, high-density specimens exposed to uniform and aggressive industrially relevant irradiation conditions to statistically quantify the uncertainty in the subsequent post-irradiation measurements. Targets RRN02, RRN04, and RRN06 aim to study UN irradiation performance at various burnup levels and irradiation temperatures. Targets RRN03 and RRN05 aim to investigate the impact of fabrication impurities and density variation on the UN irradiation performance.

Table 1. ROADRUNNER Irradiation Test Matrix

Target ID	Target temperature (°C)	Target burnup (MWd/kg U)	Fuel specimens	Testing objective
RRN01	900	75	6 UN disks	High-purity, high-density UN at high-level burnup
RRN02	600, 900, 1200	75	6 UN disks	High-purity UN at high-level burnup with variation of temperature
RRN03	900	37.5	6 UN disks	Low-level burnup with density and impurity variation
RRN04	600, 900, 1200	60	6 UN disks	High-purity UN at mid-level burnup with variation of temperature
RRN05	900	60	6 UN disks	Mid-level burnup with density and impurity variation
RRN06	600, 900, 1200	37.5	6 UN disks	High-purity UN at low-level burnup with variation of temperature

3. EXPERIMENT DESIGN AND ANALYSIS

3.1 MINIFUEL EXPERIMENT DESIGN

ROADRUNNER uses the MiniFuel design format, which has been described in the literature [3][4][5] and is pictorially represented in Figure 1. The ROADRUNNER specimen format is a UN fuel disk measuring 3 mm in diameter and 1 mm thick. Each disk specimen is placed into a molybdenum cup and inserted at the bottom of a molybdenum holder. A molybdenum filler is inserted onto the cup, which generated the majority of the sub-capsule heat from gamma rays absorption from the HFIR driver fuel. A silicon carbide (SiC) passive thermometry (TM) is placed inside the filler and is interrogated post-irradiation to verify irradiation temperature conditions. Grafoil insulators are placed on the outermost face of filler to ensure that the cup remains in contact with the holder to effectively transfer heat. Finally, a cap is welded to the holder to complete sealed sub-capsule with a 100% helium internal atmosphere. Six sub-capsules are stacked inside an irradiation target, backfilled with a mixture of helium and argon gas, and welded. The sub-capsule irradiation temperature is passively controlled by this secondary gas gap/helium and argon mixture created between the outer wall of the sub-capsule and the inner wall of the target tube. Each irradiation target is loaded into an RB MiniFuel Assembly basket at its designated radial and axial (RA) position. Sub-capsules positioning is designated by its radial-axial-sub-capsule (RAS) value (see Figure 1).

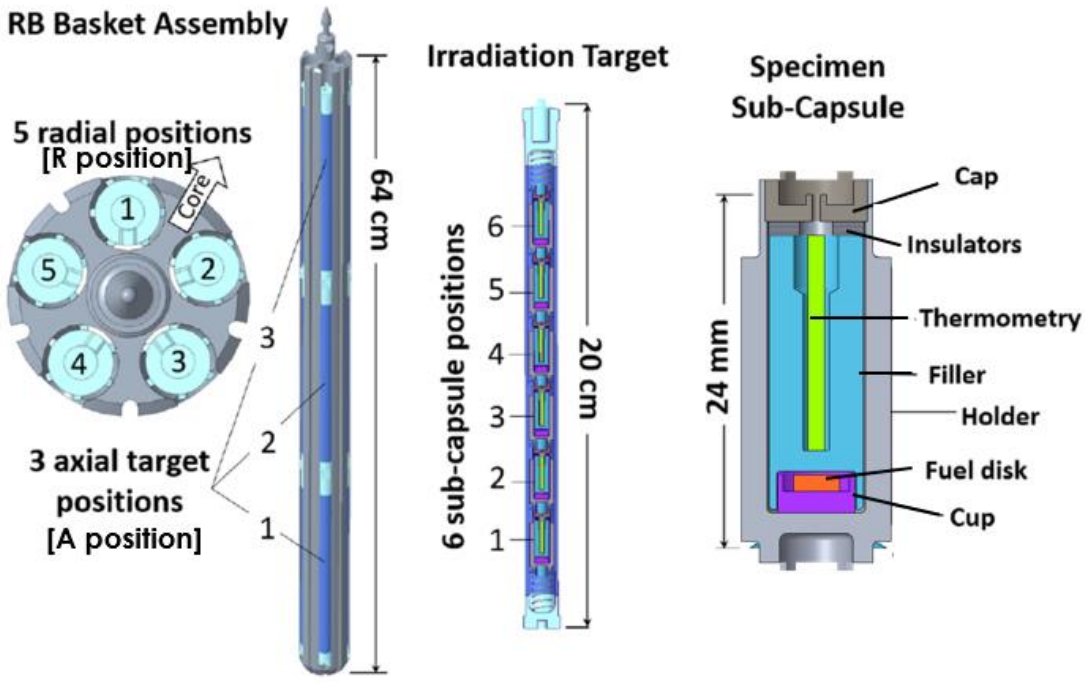

Figure 1. MiniFuel experiment design.

3.2 NEUTRONICS ANALYSIS

3.2.1 Calculation Methodology

Neutronics analyses were performed to assess the heat generation rates (HGRs) of the MiniFuel disks and target structural components. The time-dependent HGRs serve as input to the experiment thermal design (see Section 3.3). Each sub-capsule fuel burnup as a function of irradiation time was also calculated. Both the HGRs and the burnup were computed using ORNL's HFIRCON framework, which is used to simulate

reactor driver fuel and specimen depletion in HFIR. HFIRCON couples the Monte Carlo N-Particle transport code MCNP, which is used for the neutronics calculation, with SCALE's ORIGEN module, which is used to perform depletion, activation, and decay calculations. The total HGR is composed of individual heat sources that include prompt neutron, prompt photon, photons from fission product decay, local alpha and beta decay from the activated experiment, and gamma decay from target activation products. This analysis considers 25-day HFIR irradiation cycles, with a 10-day outage between cycles.

3.2.2 Model and Geometry

The MCNP model that was used in this analysis was based on previous work [4][5] and is representative of the experiment design shown in Figure 1. Figure 2 (a) shows a horizontal cross section of the HFIR neutronics model. The five MiniFuel basket radial positions R1 to R5 are azimuthally equispaced as shown in Figure 2(b). The basket radial positions R1 and R2 are equidistant from the HFIR fuel, which exposes them to a similar neutron flux. This configuration reflects the basket position when being loaded in the reactor. Radial positions R3 and R5 are also radially equivalent with respect to their neutron flux exposure. Radial position R4 is located in the back of the experiment, thus making it the farthest from the fuel region as well as the position with the least neutron flux exposure. Table 2 shows a summary of the fuel disk parameters that were used in these calculations.

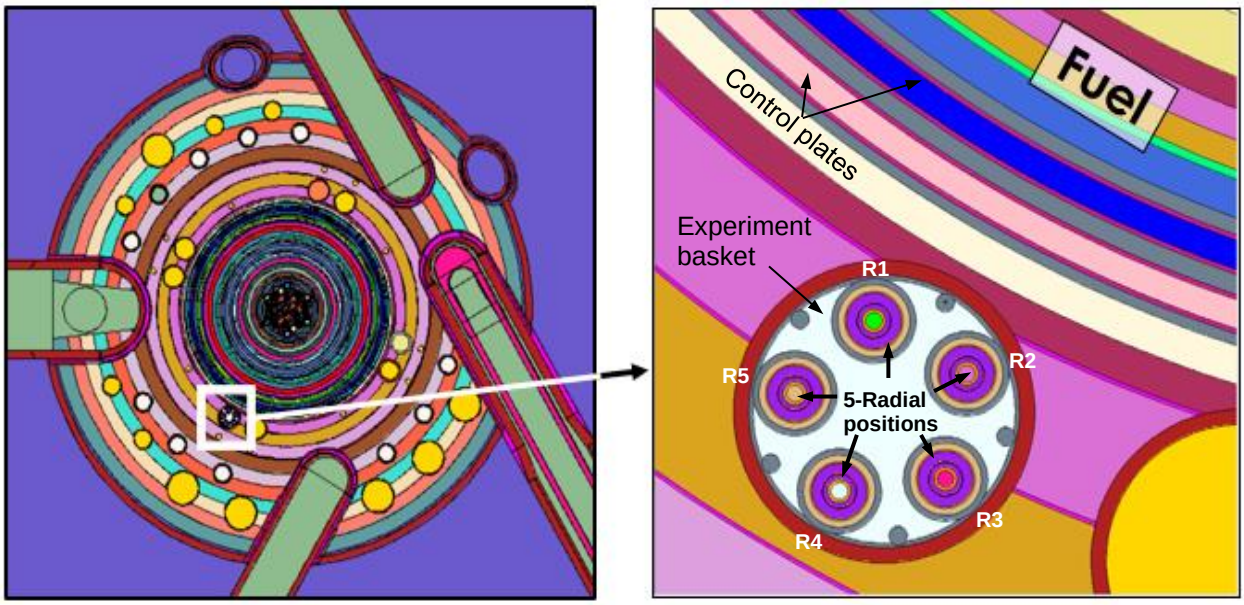

Figure 2. MCNP model of the experiment used for design analysis: (a) section view the HFIR core and (b) section view of the MiniFuel basket in position RB-5B.

Table 2. Fuel Disk Parameters Considered in the Calculation

Parameter	Calculation specification
Experiment configuration	R1 and R2 equidistant from the fuel
U-235 enrichment	0.348 wt%
Percent theoretical UN density	95%
Fuel disk outer diameter	2.9 mm
Fuel disk thickness	1.0 mm

3.2.3 Burnup Results

The burnup accumulation as a function of irradiation time was calculated for each RAS position. Figure 3 shows the burnup results simulated over a total of 15 cycles (with a cycle length of 25 days) for each sub-capsule of two targets (position RA=12 and position RA=42). The targets located in the axial midplane (A = 2) experience the highest neutron flux in the MiniFuel basket. Radial position R = 1 is one of the two radial positions closest to the HFIR fuel and thus allows for the fastest burnup accumulation. Radial position R = 4 is the radial position farthest from the core and thus provides the slowest burnup accumulation. The results show that a burnup of at least 75 MWd/kg U can be reached after 10 to 13 cycles in HFIR depending on the RAS position (with A = 2).

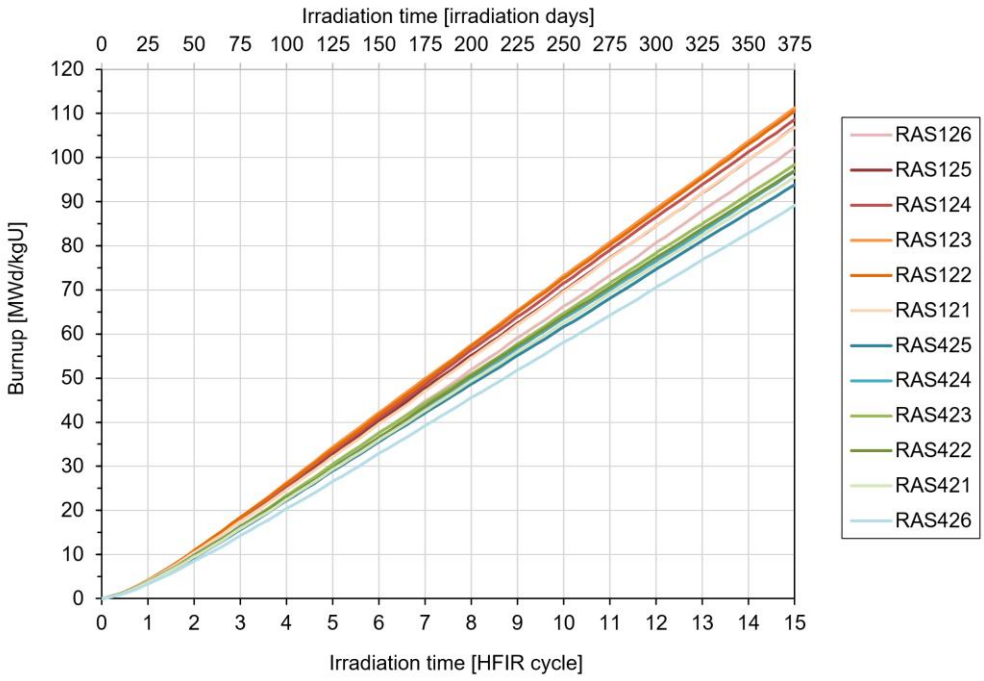

Figure 3. Fuel burnup as a function of irradiation time for several RAS positions.

3.3 THERMAL ANALYSIS

3.3.1 Calculation Methodology

The thermal design was completed utilizing ANSYS Mechanical 2023 R1, a finite element analysis software package. The CAD geometry was constructed in CREO 7 and was imported into ANSYS. The CAD geometry consists of an entire steel irradiation target with some minor features, such as welds, simplified or removed. Additionally, the springs were neglected from the model to reduce computational burden and the complexity of meshing.

Convective and coolant boundary conditions for RB MiniFuel are 24,240 W/m^2·°C (applied to the outside surface of the target) and 53.5°C coolant temperature, respectively [3][4][5]. Due to the movement of the control plates and the burnup of fuel, the heat generation rates change continuously throughout the cycle. As a result, HGRs from arbitrary discrete time steps during the irradiation are calculated via neutronics analysis and applied for each step. This serves to provide an expected fuel temperature history over the course of the irradiation. These data are linearly interpolated to provide HGRs for time steps not explicitly calculated in the neutronics analyses. Component materials and thermophysical property data assignments are listed in Table 3.

Table 3. Summary of Materials and Components

Component	Material	Property references
Target	304L stainless steel (SS)	DAC-10-16-PROP_SS304, Rev. 1 [6]
Thimbles, end cap, holder, tube, dish, springs	Molybdenum (Mo)	DAC-10-11-PROP_MOLY, Rev. 1 [7]
Thermometry	Silicon Carbide (SiC)	DAC-10-06-PROP_SIC(IRR), Rev. 3 [8]
Fuel	Uranium Nitride (UN)	DAC-16-08-PROP_UN, Rev. 0 [9]
Insulators	Grafoil	DAC-11-16-PROP_GRAFOIL, Rev. 0 [10]

The fuel disks were generally characterized as 95% dense, 0.34% enriched UN of dimensions 2.8 mm outer diameter (OD) and 1 mm height. The density variations were analyzed at 95%, 92% and 88% for 3 disk specimens in target 2, 4, and 6, with the lowest density at sub-capsule position 4 and increasing in density to position 6. These density values were based on predicted sample densities to be produced. This configuration takes advantage of the higher flux—and therefore higher heat load—at the center of the target, more easily allowing the lower density samples to reach the desired temperature.

3.3.2 Results

Specimen temperatures for all irradiation targets were calculated in this work. Prototypic average fuel temperature over an eleven-cycle HFIR irradiation in target position RA = 12 is given in Figure 4. The RA = 12 target is designed to accommodate two sub-capsules per design temperature (600, 900, and 1200°C), which are shown with the dotted lines on the plot. Each discrete drop/increase in the fuel temperature indicates the beginning of a new 25-day HFIR cycle. The HGR varies quite significantly over a cycle, with the largest change occurring during the first day. For example, the HGR of the fuel begins at ~250 W/g at day 0 and ends at ~300 W/g at day 25 of an individual cycle (RAS = 123, cycle 4). This is due to the control plate movement, which moves more quickly in the first day of operation. Additionally, the average HGR of the sample increases steadily until about the third cycle as the ^{238}U is converted to ^{239}Pu and fissions. Finally, the HGR trend increases over each cycle as the control plates are withdrawn, increasing the thermal flux in the RB position over the cycle.

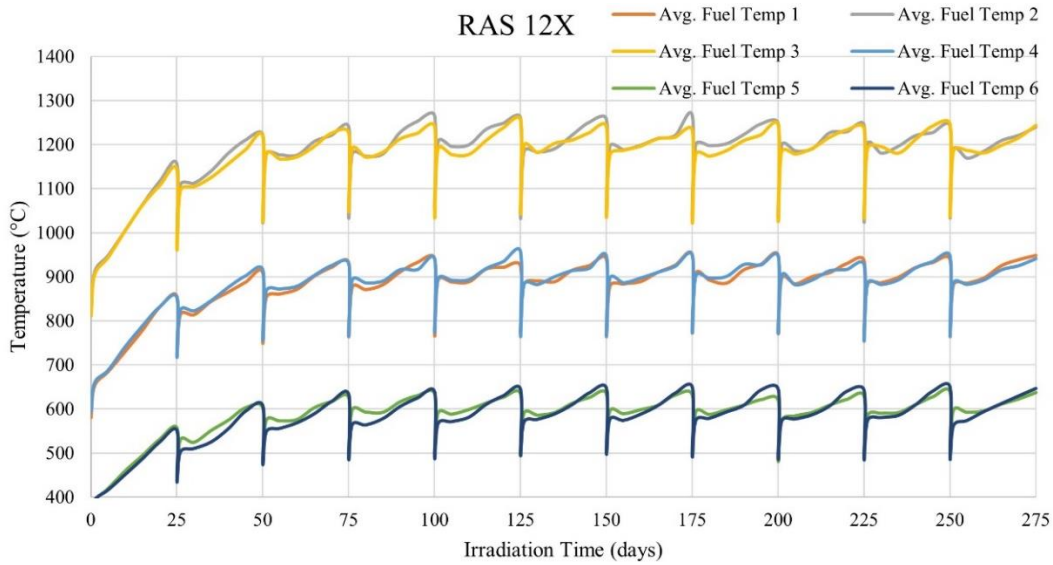

Figure 4. Evolution of the average fuel temperature for the 6 sub-capsules in position RA =12 as a function of irradiation time.

Table 4 shows the analysis results summary including the target RA location, target fill gas, target holder ODs, the time-averaged and volume-averaged (TAVA) temperatures of the fuel specimens, and the TAVA TM temperature over the final irradiation cycle. This latest data will be compared to the dilatometry data collected post-irradiation to confirm the experiment irradiation temperature [11][12]. The TAVA fuel temperatures were taken from the third cycle onward so as to account for the building HGR, and these temperatures are considered representative of the fuel specimen TAVA temperature over the entire irradiation length. Additionally, day 0 of each cycle was not included because doing so would unrealistically weight the temperatures lower. Additional temperature results, such as the minimum and maximum fuel temperature over the entire irradiation, are available in APPENDIX A. The temperature gradient in the fuel specimen is about 75°C because of the poor thermal conductivity of the fuel specimen. Figure 5 shows an example of the temperature contours of the fuel specimens (quarter model of the specimen in its cup) for the three target temperatures. Table 4 also shows the discharge burnup of each fuel specimen calculated during the neutronics analysis (see Section 3.2). Figure 6 provides a summary of the experiment TAVA fuel temperature and burnup, where each data point represents a sub-capsule. The results show that the designed MiniFuel targets agree with the irradiation conditions specified in the test matrix in Table 1.

Table 4. ROADRUNNER MiniFuel Design Summary

Target ID	Target fill gas	No. of HFIR cycles	RA location	Sub-capsule	Holder OD (mm)	TAVA fuel temperature (°C)	TAVA last cycle TM temperature (°C)	Discharge burnup (MWd/kg U)
RRN01	85% He, Ar bal.	12	42	6	9.16	917	696	70.58
				5	9.27	917	682	74.70
				4	9.36	908	663	76.57
				3	9.38	910	658	78.39
				2	9.44	890	637	77.30
				1	9.35	909	658	75.76
RRN02	85% He, Ar bal.	11	12	6	9.92	604	388	73.38
				5	9.96	608	363	77.26
				4	9.66	910	617	79.08
				3	9.18	1206	878	80.81
				2	9.13	1214	900	80.20
				1	9.68	908	641	77.16
RRN03	85% He, Ar bal.	6	32	6	9.34	911	684	34.98
				5	9.40	914	678	36.81
				4	9.43	908	675	37.41
				3	9.54	899	639	38.52
				2	9.49	914	655	38.42
				1	9.49	908	650	37.40
RRN04	85% He, Ar bal.	9	22	6	9.92	602	388	59.36
				5	9.96	608	362	62.29
				4	9.67	899	610	63.99
				3	9.18	1210	877	65.17
				2	9.11	1217	906	64.51
				1	9.69	902	634	62.37
RRN05	85% He, Ar bal.	9	52	6	9.32	918	691	54.85
				5	9.41	910	674	57.51
				4	9.44	910	672	59.85
				3	9.52	906	646	59.90
				2	9.51	909	646	59.83
				1	9.50	902	642	58.63
RRN06	85% He, Ar bal.	6	12	6	9.92	604	389	37.57
				5	9.96	608	364	40.27
				4	9.66	910	620	40.96
				3	9.18	1206	882	42.17
				2	9.13	1214	905	41.63
				1	9.68	908	642	39.58

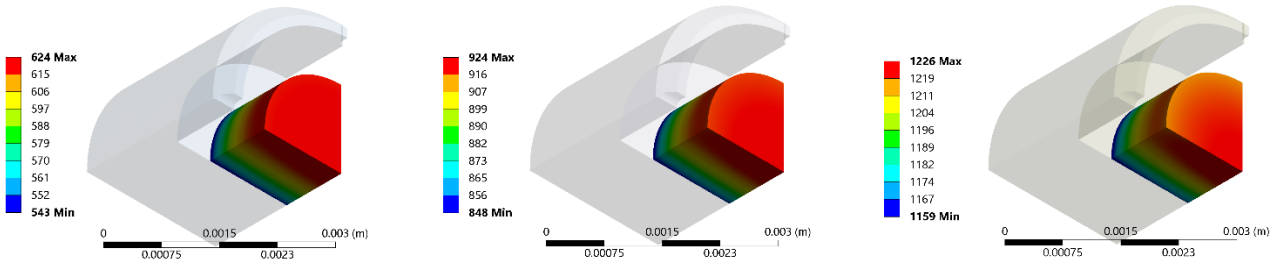

(a) (b) (c)

Figure 5. Temperature distribution in the fuel specimen for designed average temperature of (a) 600°C, (b) 900°C, and (c) 1200°C.

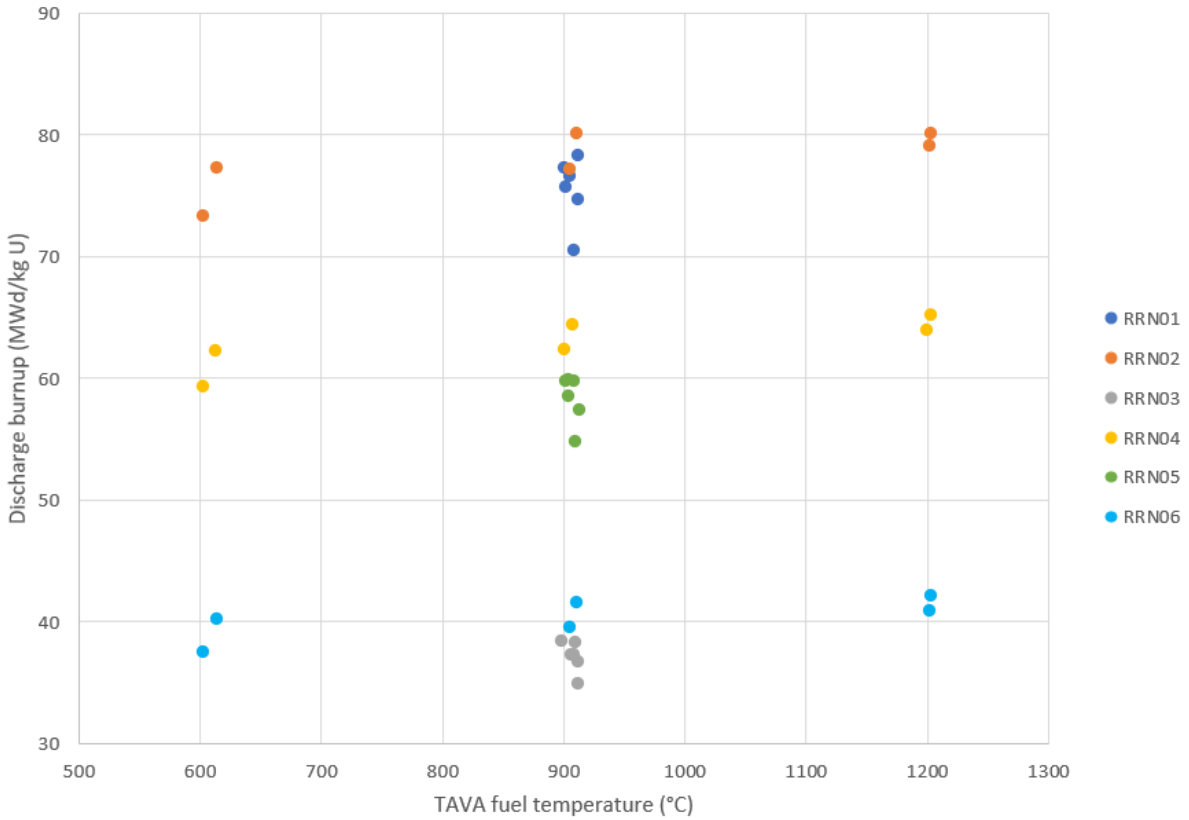

Figure 6. Distribution of TAVA fuel temperatures and discharge burnups.

4. SPECIMEN CHARACTERIZATION

Depleted UN fuel specimens were chosen for this experiment to facilitate handling and shipping of the specimens. The UN specimens were fabricated by LANL via carbo-thermic reduction following nitriding/denitriding (CTRN), and were metallurgically thinned down to their desired geometry by UTSA. The uranium feedstock used for this fabrication was also used previously in the fabrication of UO_2 specimens, and its isotopic composition was analyzed at the time of this previous fabrication (see APPENDIX B). X-ray diffraction (XRD) was performed at LANL to verify the phases present in each furnace batch. APPENDIX C shows as an example the XRD results for batch 24-006-MF, compared to expected UN XRD results from the Inorganic Crystal Structure database [13]. These results confirm the UN nature of the furnace batch.

The UN samples were categorized based on fabrication batches from LANL, with classifications for density (high, mid, or low) and purity (high purity/low carbon, mid carbon, high carbon). The density of selected pellets was calculated at LANL upon fabrication from geometric and mass measurements. The density was similarly calculated on selected disk specimens at UTSA upon grinding, and at ORNL upon specimen inspection. The inspected specimens met the dimensions required for HFIR irradiation. The density results are detailed in APPENDIX D, where the density is specified in percentage of the theoretical density (TD=14.32 g/cc). The densities calculated by each institution for the various batches are within standard deviation of each other's. Carbon and oxygen contents were measured by LANL by combustion analysis using a LECO C844 series. The results are presented in APPENDIX D, and show three distinct levels of carbon impurities (low – i.e. high purity, mid, and high).

Microstructure analysis of the specimens was collected by UTSA after the sample thinning process, and the results (as available at the time of this writing) are presented in APPENDIX E. The overall observed microstructure demonstrates that the fuel samples are composed of a homogeneous grain distribution, and no secondary phases (such as oxides) were observed. The high-density samples show only closed pores (within the grains), whereas the low-density samples exhibit open pores, which are interconnected with the grain boundaries. Figure 7 summarizes the characteristics of the different fuel batches.

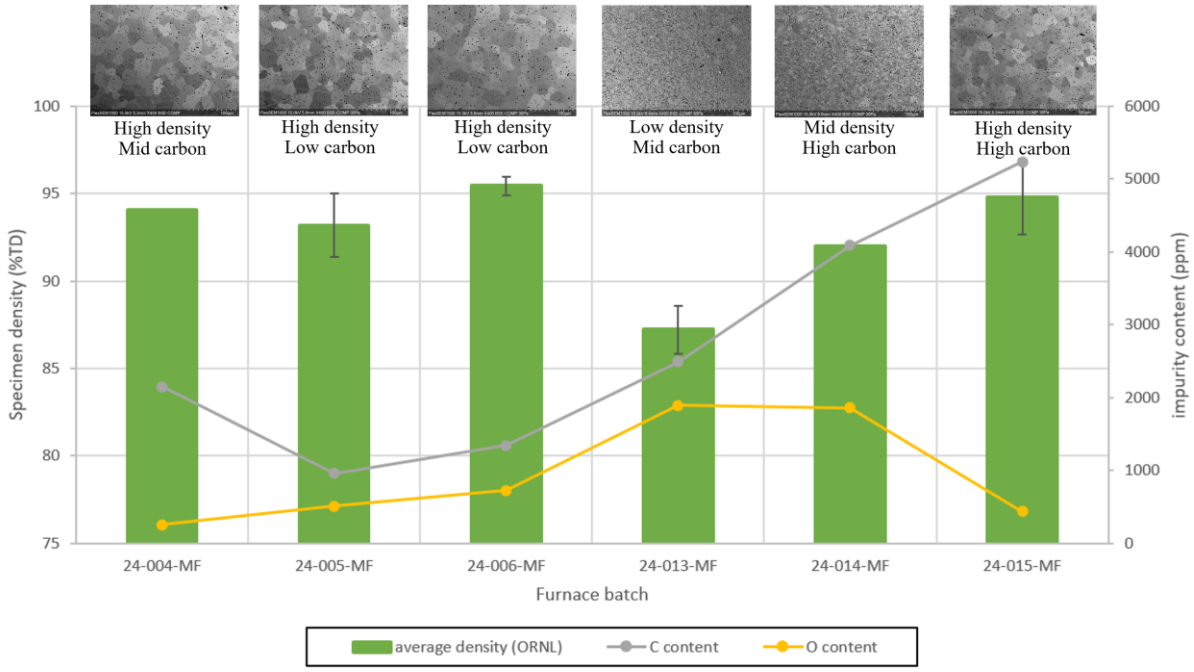

Figure 7. Summary of the fuel batches characteristics.

X-ray computed tomography (XCT) was performed on selected specimens to measure their volume and to identify any features of interest within the samples. XCT was performed using a Versa 620 system operating with an accelerating voltage of 160kV at 25W with an HE2 filter to remove low energy x-rays which would not contribute to the image due to strong x-ray attenuation by the uranium-bearing sample. A total of 1601 radiographs distributed evenly over 360° of rotation were acquired for each specimen with an exposure time of 10s per radiograph. The 4x objective in the Versa 620 was used with x-ray source and detector positioned such that the voxel edge length was 1.91μm. Radiographs were reconstructed into a 3D tomogram using the standard Zeiss reconstruction software with a beam hardening constant of 0.25 to reduce uneven brightness from the sample edge to center due to hardening of the x-ray spectrum.

Example tomographs from different perspectives of specimen 35-P-24-073 are shown in Figure 8. As may be seen in these images, there are some darker regions internal to the sample. These dark regions represent areas with lower x-ray attenuation than the bulk sample, and may correspond to pores, cracks, or potentially low-Z inclusions. Minor cracks are expected on the grinded surface of the specimens and do not appear on the opposite surface of the specimens. In agreement with the measured density, the specimen is observed to be high density with no major crack or defect.

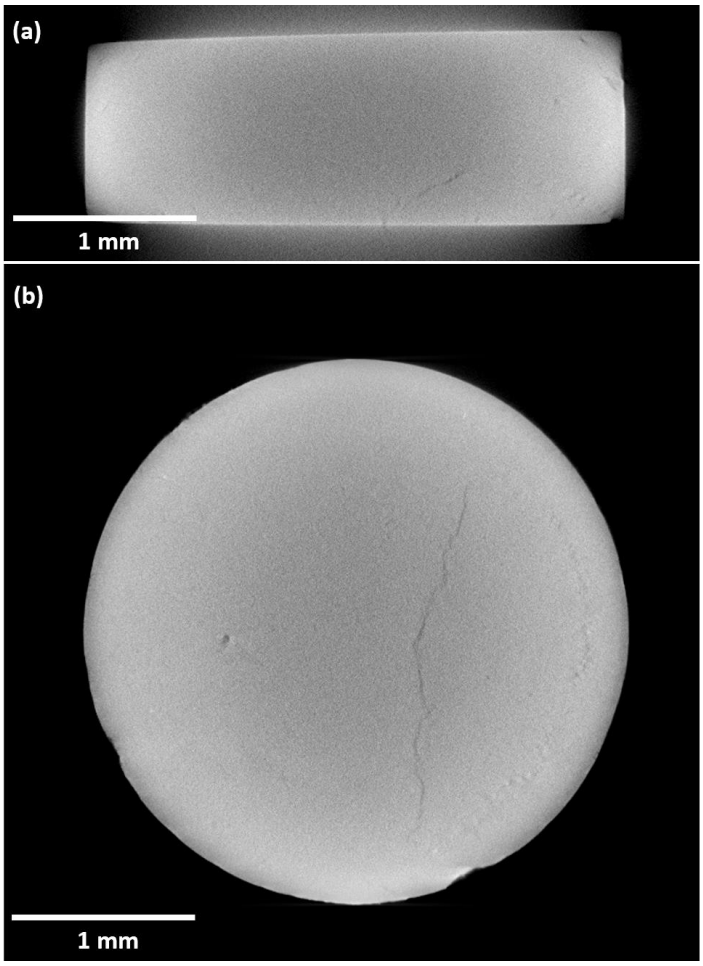

Figure 8. Tomographic slices showing (a) side view and (b) top-down view from XCT image of specimen 35-P-24-073. Dark regions within the disk correspond to pores, cracks, or other low-Z features which attenuate fewer x-rays.

The volume of XCT imaged specimens was determined by processing the data in MATLAB. The native 16-bit images were converted to 8-bit for ease of processing, then a 3D median filter was applied to the images to reduce the impact of random noise and speckling. Locally adaptive 3D thresholding was then used to segment the sample from the background based on local variations in image intensity. This initial segmentation was refined by morphological closing and filling operations to produce a single, solid object. Finally, the total number of voxels in the segmented object was used along with the known voxel volume to calculate the total sample volume. In the case of sample 35-P-24-073, a total volume of 7.1249 mm^3 was calculated. An assessment of the uncertainty associated with this measurement based on the local gradients in image intensity near the sample edges remains to be performed.

5. FUTURE WORK

The six ROADRUNNER targets, each consisting of 6 sub-capsules, will be assembled, tested, and welded according to HFIR-approved procedures, drawings, and sketches. Following full approval, the targets will be inserted in HFIR. Table 5 shows the irradiation timeline for each ROADRUNNER target. The HFIR insertion for all the targets is expected to be done on a staggered timeline to accommodate the positions' availability in the MiniFuel basket.

Table 5. Irradiation Plan for the ROADRUNNER Targets

Target ID	RA position	No. of HFIR irradiation cycles	Target insertion cycle	Target end of irradiation
RRN01	42	12	Cycle 510 (October 2024)	Cycle 521 (October 2026)
RRN02	12	11	Cycle 512 (April 2025)	Cycle 522 (July 2027)
RRN03	32	6	Cycle 510 (October 2024)	Cycle 515 (December 2025)
RRN04	22	9	Cycle 511 (February 2025)	Cycle 519 (August 2026)
RRN05	52	9	Cycle 511 (February 2025)	Cycle 519 (August 2026)
RRN06	12	6	Cycle 511 (February 2025)	Cycle 516 (January 2026)

After HFIR irradiation, the targets will be shipped to ORNL's Irradiated Fuels Examination Laboratory (IFEL) for disassembly and post-irradiation examination (PIE). PIE on the fuel specimens includes fission gas release measurements, visual inspection, fuel swelling measurements, gamma spectroscopy, and microstructure analysis. The TMs will be shipped from IFEL to the Low-Activation Materials Development and Analysis Laboratory to be analyzed via dilatometry to confirm the irradiation temperature [10][12]. The dilatometry results will be compared to the TAVA TM temperature over the last irradiation cycle (see Table 4).

6. REFERENCES

[1] Matthews, R.B., Irradiation performance of nitride fuels. 1993, Los Alamos National Lab., NM (United States).

[2] Wallenius, J., Nitride Fuels, in Comprehensive Nuclear Materials, R.J. Konings and R. Stoller, Editors. 2020, Elsevier.

[3] Jacob P. Gorton, Annabelle G. Le Coq, Zane G. Wallen, Christian M. Petrie, Joshua T. White, John T. Dunwoody, Shane Mann, Nathan A. Capps, Andrew T. Nelson, "Modeling and design of a separate effects irradiation test targeting fission gas release from Cr-doped UO_2," submitted to Nuclear Engineering and Design (under review) (2024).

[4] Petrie, C.M., J.R. Burns, A.M. Raftery, A.T. Nelson, and K.A. Terrani, "Separate effects irradiation testing of miniature fuel specimens," Journal of Nuclear Materials, 2019. 526:p. 151783.

[5] J.P. Gorton, Z. G. Wallen, C. M. Petrie, Modifications to MiniFuel Vehicle to Enable Higher Temperature UO_2 Irradiation Capabilities, ORNL/SPR-2021/2096, Oak Ridge National Laboratory, Oak Ridge, TN, August 2021.

[6] McDuffee, J.L., *Thermophysical Properties for 304 Stainless Steel*, DAC-10-16-PROP_SS304, Rev. 1, Oak Ridge National Laboratory: Oak Ridge, TN, 2013.

[7] McDuffee, J.L., *Thermophysical Properties for Molybdenum*, DAC-10-11-PROP_MOLY, Rev. 1, Oak Ridge National Laboratory: Oak Ridge, TN, 2013.

[8] McDuffee, J.L., Thermophysical Properties for Irradiated Silicon Carbide, DAC-10-06-PROP_SIC(IRR), Rev. 3, Oak Ridge National Laboratory: Oak Ridge, TN, 2013.

[9] Petrie, C.M., Thermophysical Properties for Uranium Nitride, DAC-16-08-PROP_UN, Rev. 0, Oak Ridge National Laboratory: Oak Ridge, TN, 2017.

[10] McDuffee, J.L., Thermophysical Properties for Flexible Graphite, DAC-11-16-PROP_GRAFOIL, Rev. 0, Oak Ridge National Laboratory: Oak Ridge, TN, 2013.

[11] A.A. Campbell, W.D. Porter, Y. Katoh, L.L. Snead, "Method for analyzing passive silicon carbide thermometry with a continuous dilatometer to determine irradiation temperature," Nuclear Instruments and Methods in Physics Research B, 370 (2016).

[12] K.G. Field, J.L. McDuffee, J.W. Geringer, C.M. Petrie, Y. Katoh, "Evaluation of the continuous dilatometer method of silicon carbide thermometry for passive irradiation temperature determination," Nuclear Instruments and Methods in Physics Research B, 445 (2019).

[13] D. Zagorac, H. Muller, S. Ruehl, J. Zagorac, S. Rehme, "Recent developments in the Inorganic Crystal Structure Database: theoretical crystal structure data and related features," Journal of Applied Crystallography, 52 (2019).

APPENDIX A. ADDITIONAL FUEL AND TM TEMPERATURES

APPENDIX A. ADDITIONAL FUEL AND TM TEMPERATURES

Target ID	RA position	Temperature (°C)	Sub-capsule position					
			1	2	3	4	5	6
RRN01	42	Max. Fuel	974	953	968	972	991	995
		Min. Fuel	863	813	833	830	838	832
		TAVA SiC	662	641	662	667	684	698
		Max. SiC	691	667	688	696	717	738
RRN02	12	Max. Fuel	976	1288	1277	981	670	680
		Min. Fuel	855	1122	1129	829	516	508
		TAVA SiC	642	904	881	620	364	389
		Max. SiC	673	907	891	628	370	396
RRN03	32	Max. Fuel	971	977	958	968	983	987
		Min. Fuel	862	847	828	837	841	824
		TAVA SiC	650	655	639	676	679	684
		Max. SiC	675	680	662	702	708	720
RRN04	22	Max. Fuel	961	1293	1273	967	673	679
		Min. Fuel	849	1137	1127	820	524	511
		TAVA SiC	636	910	881	613	364	389
		Max. SiC	664	937	917	641	383	415
RRN05	52	Max. Fuel	966	972	965	977	979	1006
		Min. Fuel	854	834	831	839	833	830
		TAVA SiC	645	648	648	673	676	692
		Max. SiC	670	673	672	699	706	728
RRN06	12	Max. Fuel	976	1288	1277	981	670	680
		Min. Fuel	855	1122	1129	829	516	508
		TAVA SiC	642	904	881	620	364	389
		Max. SiC	673	907	891	628	370	396

APPENDIX B. URANIUM ISOTOPICS

APPENDIX B. URANIUM ISOTOPICS

Los Alamos NATIONAL LABORATORY EST. 1943

C3Lab Chemical Certification & Compatibility LABORATORY

To: Scarlett Paisner, Josh White, Adrien Terricabras
From: Beth Judge and Keri Campbell
Phone: 5-8778
Date: June 27, 2023

SUBJECT: ISOTOPIC ANALYSIS OF UO_2 SAMPLE VIA ICP-MS

One uranium sample, ARV-81-red, was submitted for isotopic analysis. The sample was digested then diluted and isotopic composition was measured.

Sample Preparation

The uranium oxide sample was weighed in a pre-tared PFA container. Five milliliters of Optima Grade concentrated nitric acid (CAS No. 7697-37-2) was added to the sample and heated to 80ºC. After 30 minutes all of the solid uranium was digested. After cooling the uranium solutions, they were diluted by a factor of 4,000,000 for ICP-MS isotopic analysis.

A uranium isotopic Certified Reference Material (New Brunswick Laboratory, CRM U005A) was also prepared for validation of the isotopic measurement. The certified atomic percent of ^{235}U in CRM U005A is 0.5064%.

ICP Analysis Discussion
Uranium Isotopic Composition

A Thermo iCAP ICP-MS was used to analyze the standards (elemental and isotopic), sample, and QCs. The instrument was tuned following the User's Manual Operating Procedure. A passing performance report was obtained ensuring working order of the instrument. The nebulizer gas flow rate was set to 0.80 L/min and the plasma power was 1550 W. The instrument parameters for the uranium isotopes were as follows: standard measurement mode, 200 sweeps per isotope, and dwell times of 0.1, 0.1, 0.1, and 0.01 seconds for ^{234}U, ^{235}U, ^{236}U, and ^{238}U, respectively. Each sample was measured in ten replicates.

Uranium isotopic composition was validated using an isotopic CRM from New Brunswick Laboratory. The CRM is analyzed in the same experiment, under the same conditions as the sample. This analysis yielded a measured ^{235}U atomic percent of 0.5096 ± 0.0020%. Comparing the results for the certified ^{235}U atomic percent of 0.5064%, the percent difference from theoretical (theoretical – measured/theoretical) is -0.62% which is very low. This result validates the method is accurate and precise for measurements of ^{235}U atomic percent in the range of interest for the unknown sample. We applied the isotopic correction for ^{235}U and ^{236}U to account for the slight deviation between the certified value and the measured value. The ^{235}U atomic percent was calculated for each of the 10 replicates and the average of the replicates is reported in Table 1. The precision of the measurement is highlighted by the very low standard deviation.

Isotope	^{234}U at. %	^{235}U at. %	^{236}U at. %	^{238}U at. %
NBL CRM U005A Certified Values	0.0034 ± 0.00007	0.5064 ± 0.0003	0.00118± 0.00001	99.489 ± 0.0003
NBL CRM U005A Measured Values	0.0034 ± 0.0001	0.5096 ± 0.0020	0.00134± 0.00006	99.486 ± 0.002
ARV-81-red	0.0020 ± 0.0001	0.3447 ± 0.0025	0.00314± 0.00004	99.651 ± 0.002

Table 1: Certified Reference Material U005A from New Brunswick Laboratory comparing the certified and measured values along with the results from the uranium oxide sample.

APPENDIX C. XRD OF HIGH PURITY UN POWDER FEEDSTOCK

APPENDIX C. XRD OF HIGH PURITY UN POWDER FEEDSTOCK

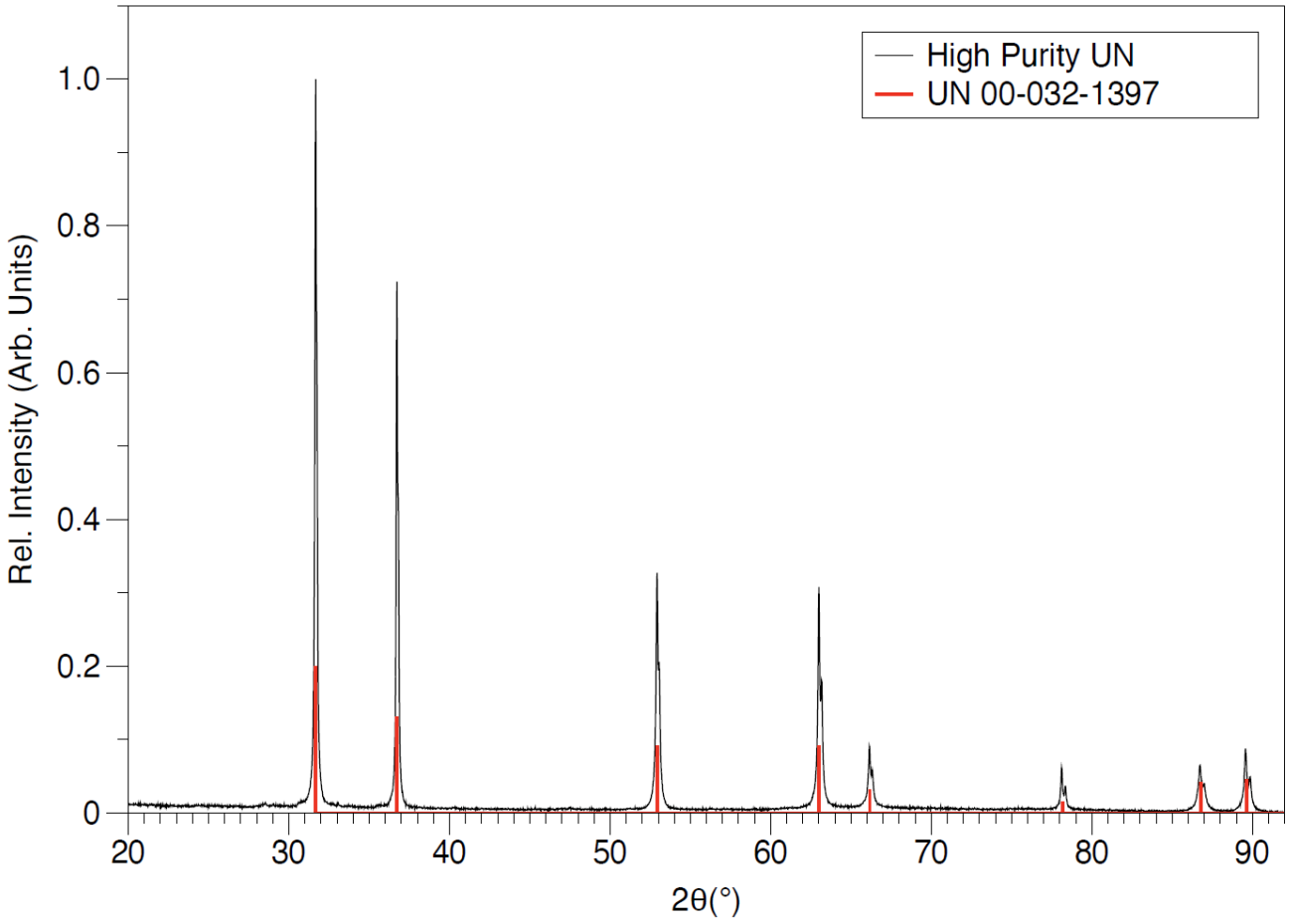

X-Ray diffraction of high purity UN feedstock (24-006-MF) used for pellet production

APPENDIX D. CHARACTERISTICS OF FUEL PELLETS AND MINIFUEL SPECIMENS

APPENDIX D. CHARACTERISTICS OF FUEL PELLETS AND MINIFUEL SPECIMENS

Batch ID	Testing objective	Pellet/ Specimen ID	Individual density			Batch density			Impurity level	
			LANL	UTSA	ORNL	LANL	UTSA	ORNL	O	C
			(%TD)			(%TD)			(ppm)	
24-004-MF	High density, Mid carbon	35-P-24-041	95.15			95.15	97.09 (σ = 1.09)	94.07	255	2150
		35-P-24-042	95.15	96.09	94.07					
		35-P-24-043		96.17						
		35-P-24-044		94.95						
		35-P-24-045		97.26						
		35-P-24-047		97.30						
		35-P-24-048		96.36						
		35-P-24-049		97.65						
		35-P-24-050		98.39						
		35-P-24-051		98.28						
		35-P-24-052		97.30						
		35-P-24-053		98.28						
24-005-MF	High density, high purity	35-P-24-063	95.25	97.58		95.28 (σ = 0.13)	95.48 (σ = 2.29)	93.20 (σ = 1.80)	507	961
		35-P-24-064	95.42	95.01	94.73					
		35-P-24-065	95.17	89.85	88.79					
		35-P-24-066		94.95	93.43					
		35-P-24-067		97.58	94.21					
		35-P-24-068		96.03	92.89					
		35-P-24-069		92.44						
		35-P-24-070		96.14	92.00					
		35-P-24-071		95.36	93.19					
		35-P-24-072		97.35	94.10					
		35-P-24-073		96.69	95.14					
		35-P-24-076		96.71	93.48					
24-006-MF	High density, high purity	35-P-24-079	96.93			96.17 (σ = 0.96)	97.90 (σ = 1.17)	95.44 (σ = 0.52)	725	1340
		35-P-24-080	95.09	97.36	95.76					
		35-P-24-081	96.47	96.82	95.21					
		35-P-24-082		97.90	94.33					
		35-P-24-083		98.59						
		35-P-24-084		96.35	95.45					
		35-P-24-085		99.43	96.14					
		35-P-24-086		99.87	95.43					
		35-P-24-087		99.20	95.49					
		35-P-24-088		98.26	95.63					
		35-P-24-089		96.77	94.79					
		35-P-24-090		97.52	95.59					
		35-P-24-091		96.79	96.05					
24-013-MF	Low density, mid carbon	35-P-24-145	88.40			88.53 (σ = 0.25)	89.58 (σ = 1.60	87.23 (σ = 1.36)	1890	2490
		35-P-24-146	88.90							
		35-P-24-147	88.40	91.17						
		35-P-24-148	88.40	90.56	88.19					
		35-P-24-149		88.50						
		35-P-24-150		87.17	86.27					
		35-P-24-151		89.05						
		35-P-24-152		91.02						
24-014-MF	Mid density, high carbon	35-P-24-158	91.60			91.60	92.96 (σ = 0.95)	91.99	1860	4090
		35-P-24-159	91.60							
		35-P-24-160		92.59						
		35-P-24-161		94.87	91.99					
		35-P-24-162		92.50						
		35-P-24-163		92.40						
		35-P-24-164		92.89						
		35-P-24-165		92.50						

Batch ID	Testing objective	Pellet/ Specimen ID	Individual density			Batch density			Impurity level	
			LANL	UTSA	ORNL	LANL	UTSA	ORNL	O	C
			(%TD)			(%TD)			(ppm)	
24-015-MF	High density, high carbon	35-P-24-166	95.12			94.70 (σ = 0.59)	95.81 (σ = 1.37)	94.80 (σ = 2.16)	436	5240
		35-P-24-167	94.28							
		35-P-24-168		97.16						
		35-P-24-170		95.88	96.32					
		35-P-24-171		96.76						
		35-P-24-172								
		35-P-24-173		93.52	93.27					
		35-P-24-174		96.63						
		35-P-24-175		94.95						

APPENDIX E. SEM IMAGES OF THE FUEL SPECIMENS

APPENDIX E. SEM IMAGES OF THE FUEL SPECIMENS

Batch 24-004-MF

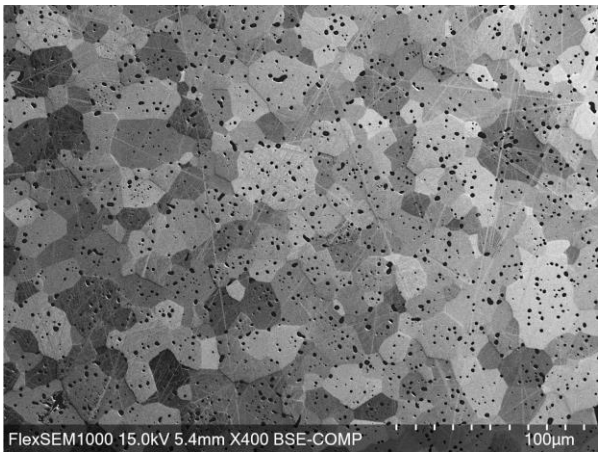

35-P-24-042

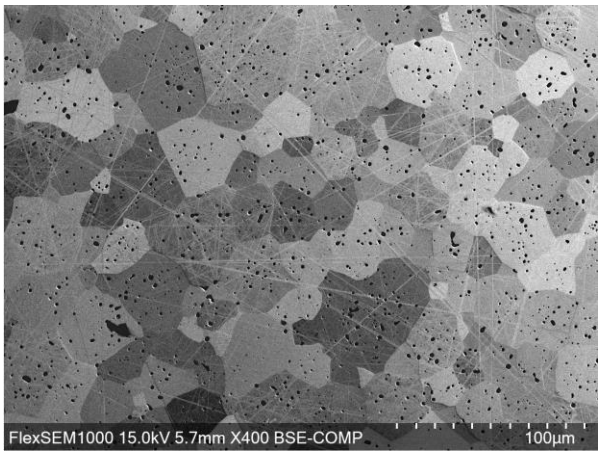

35-P-24-043

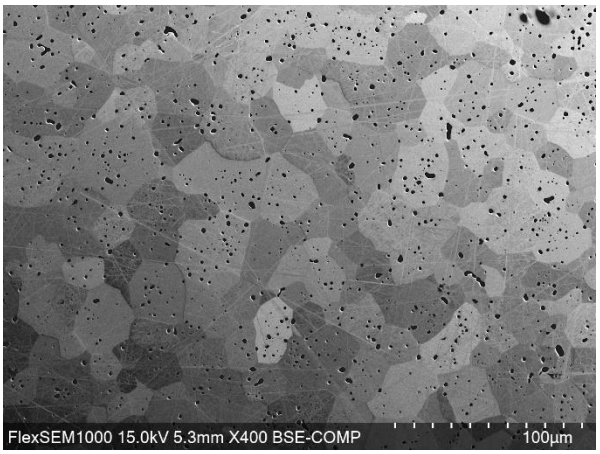

35-P-24-044

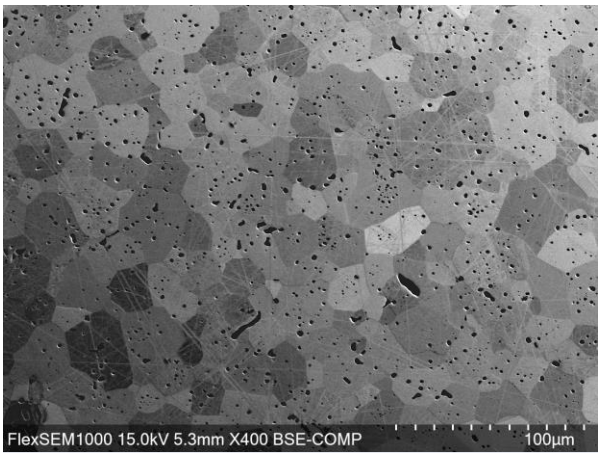

35-P-24-045

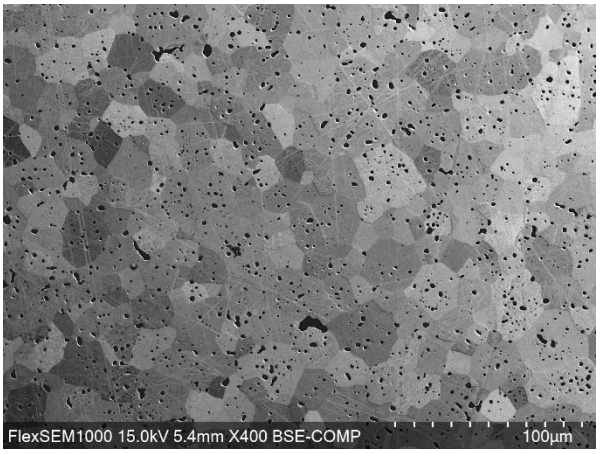

35-P-24-047

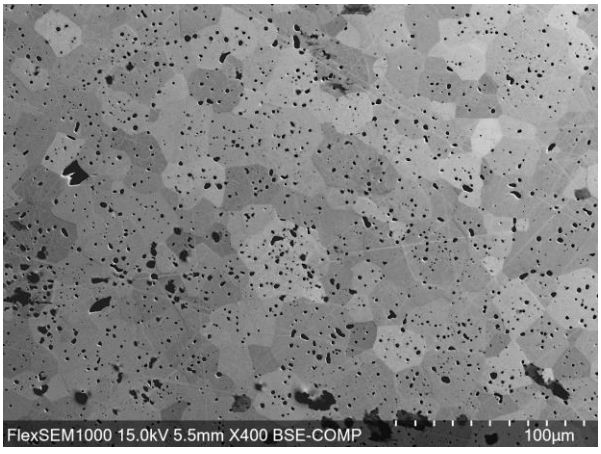

35-P-24-048

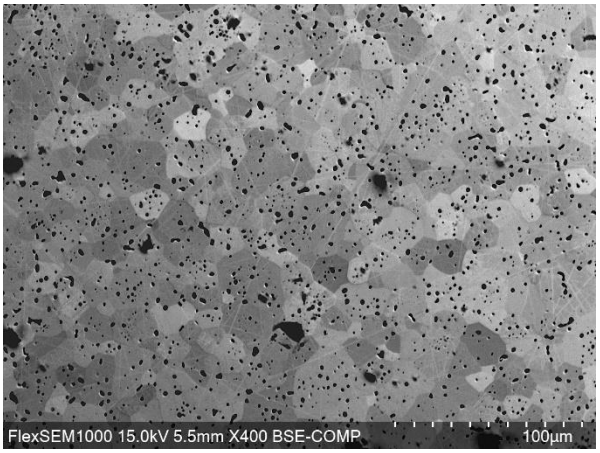

35-P-24-049

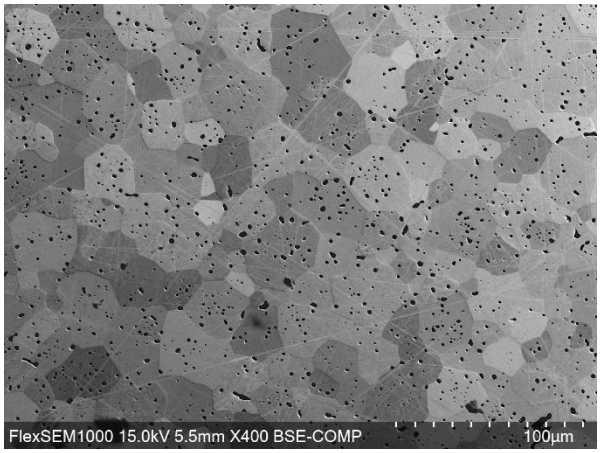

35-P-24-050

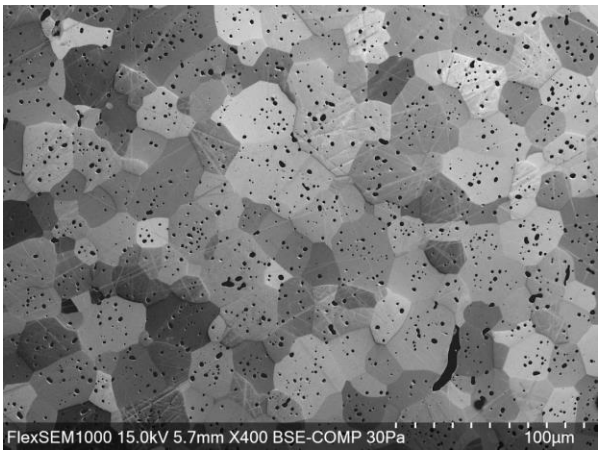

35-P-24-051

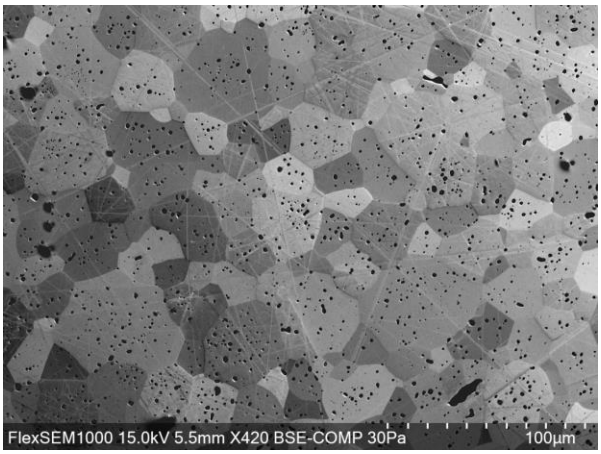

35-P-24-052

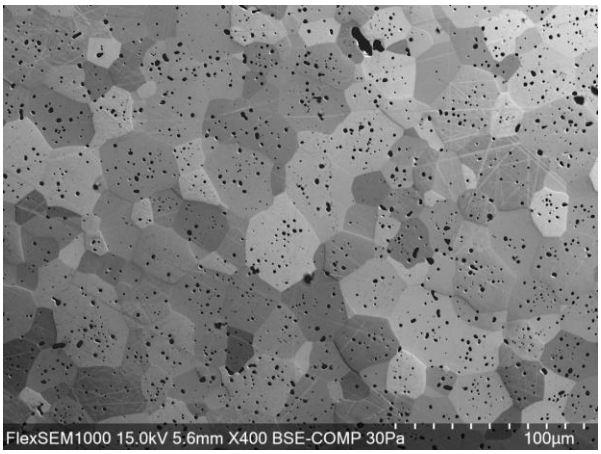

35-P-24-053

Batch 24-005-MF

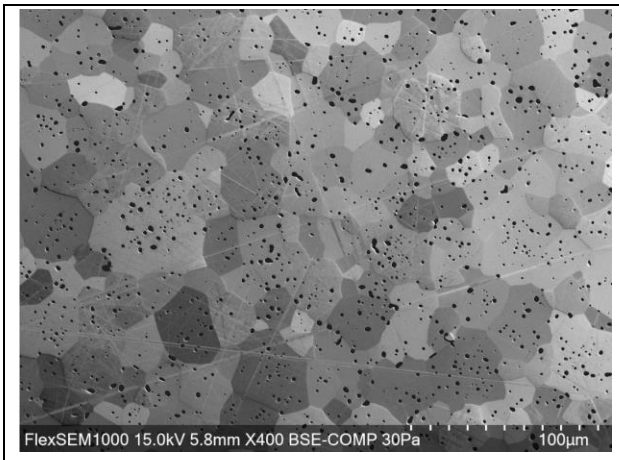

35-P-24-063

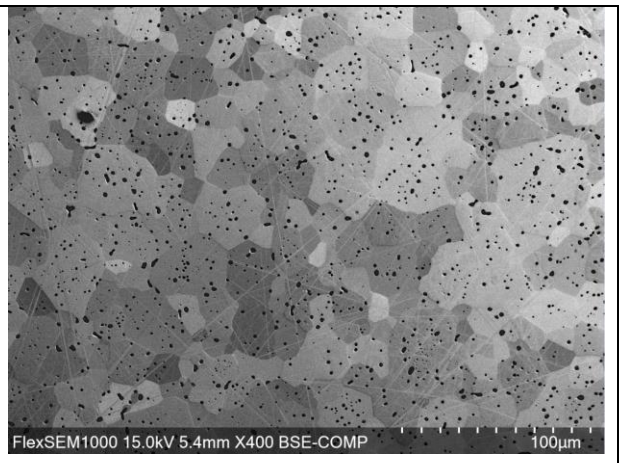

35-P-24-064

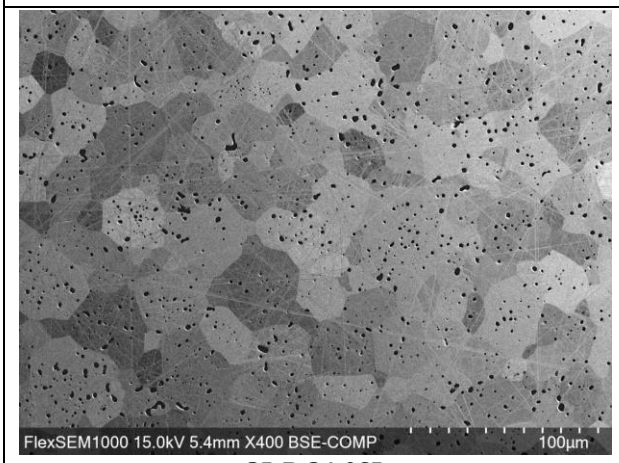

35-P-24-065

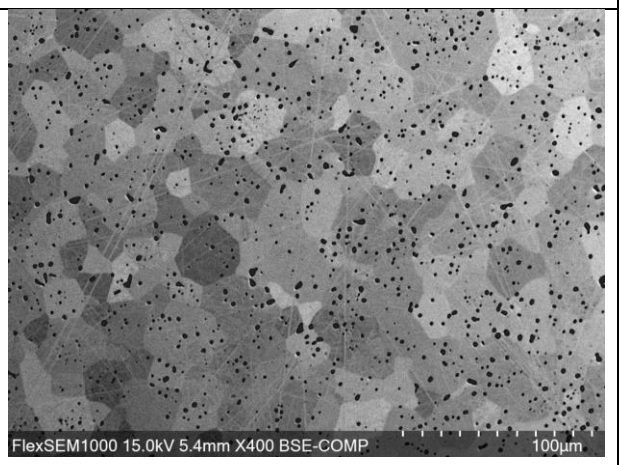

35-P-24-066

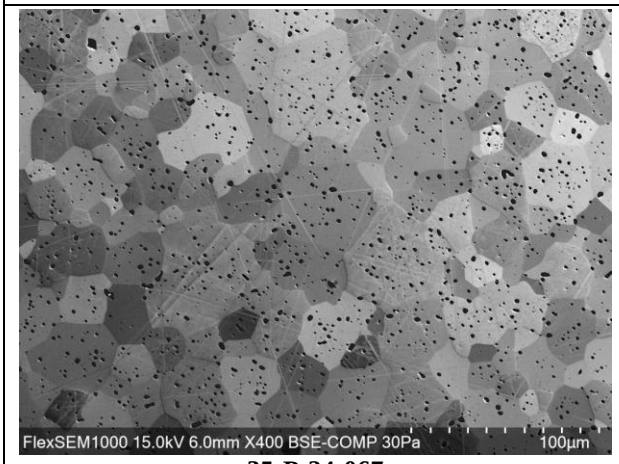

35-P-24-067

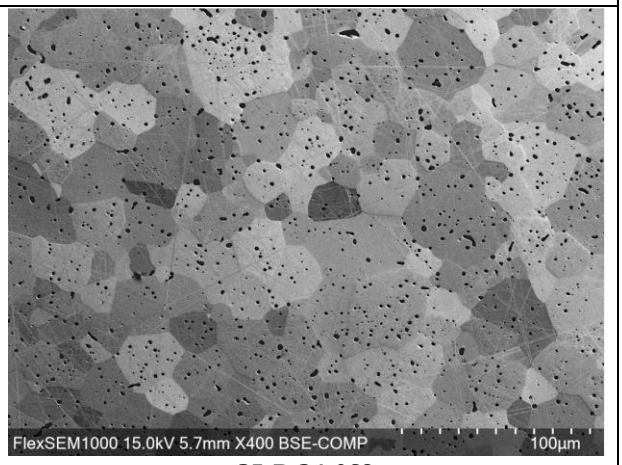

35-P-24-068

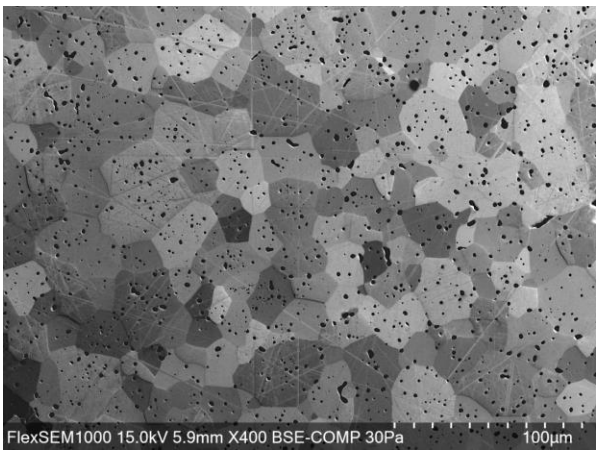

35-P-24-069

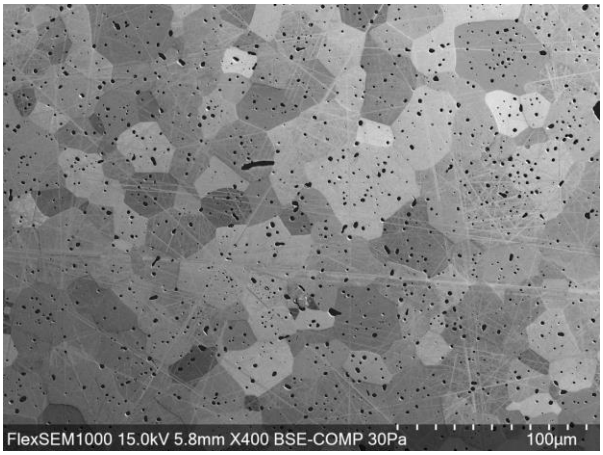

35-P-24-070

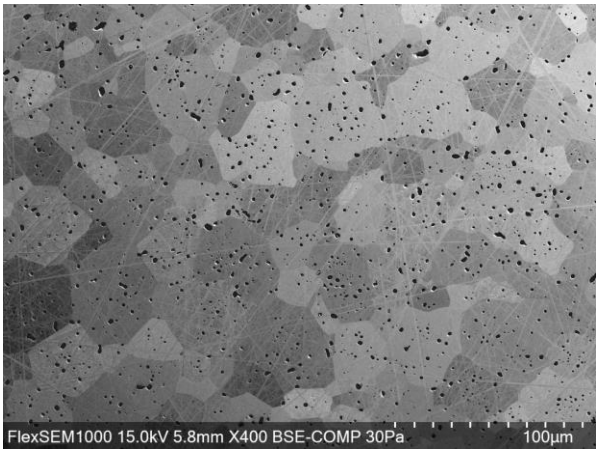

35-P-24-071

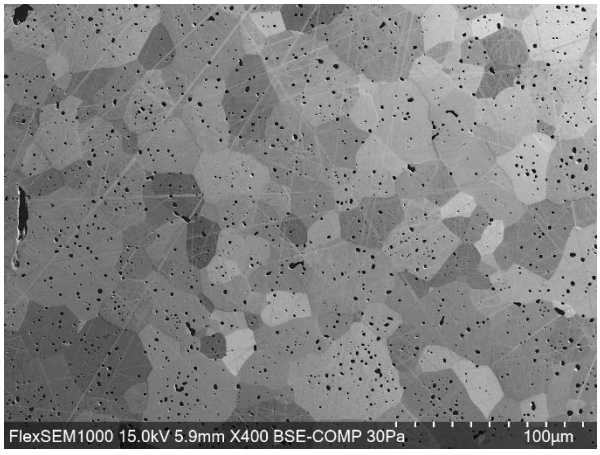

35-P-24-072

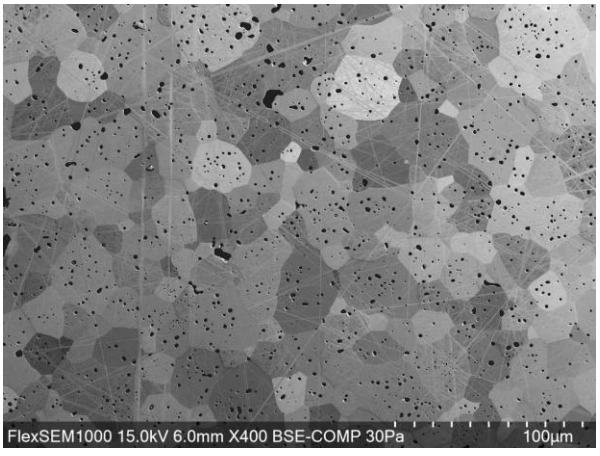

35-P-24-073

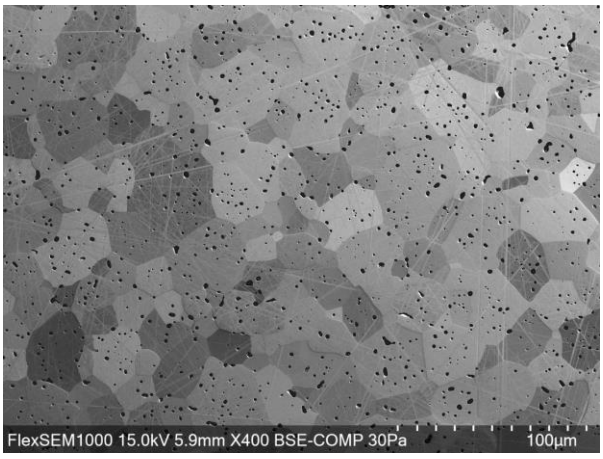

35-P-24-076

Batch 24-006-MF

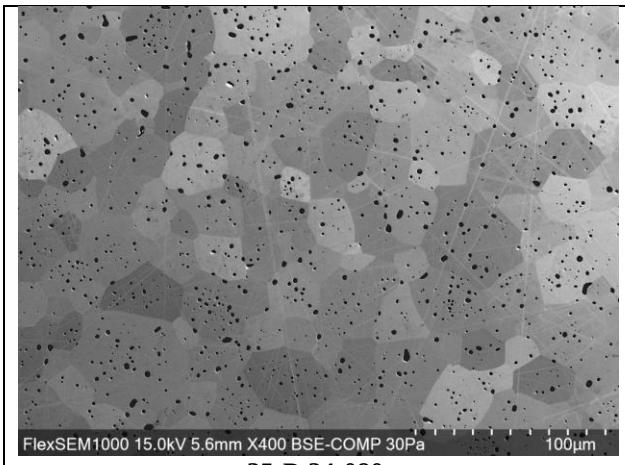

35-P-24-080

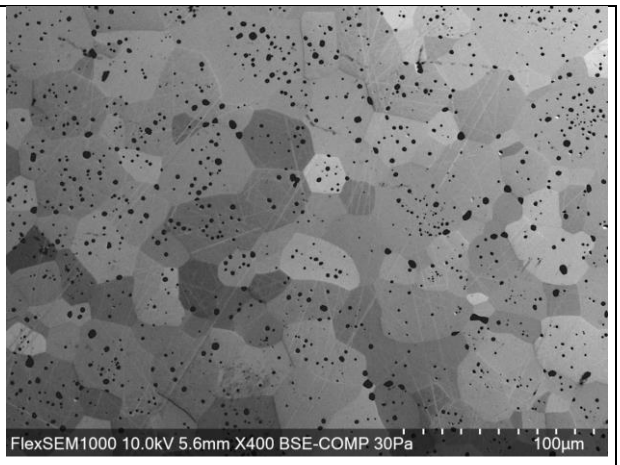

35-P-24-081

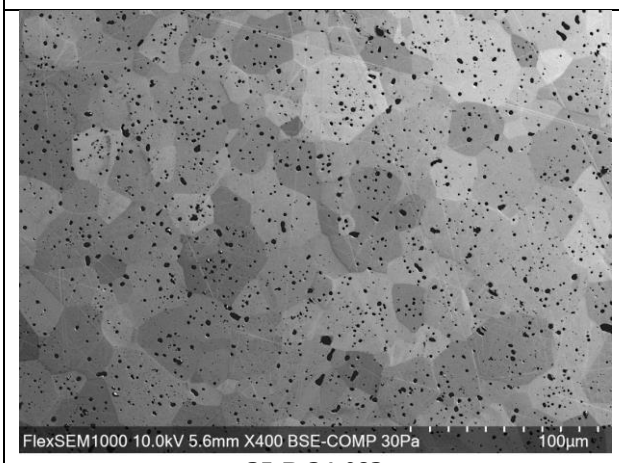

35-P-24-082

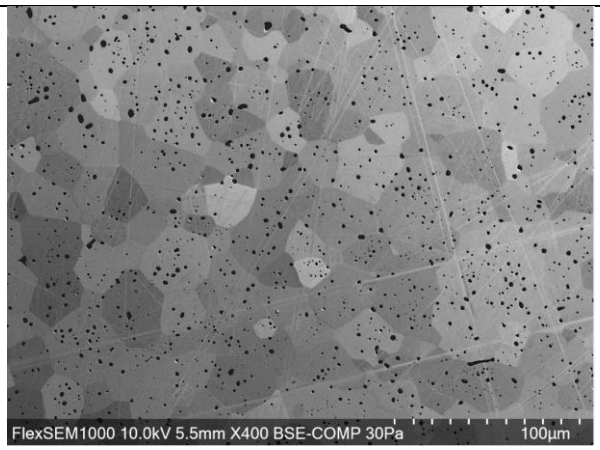

35-P-24-083

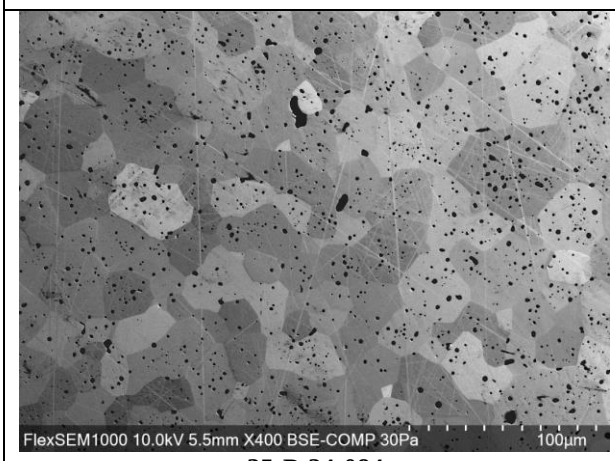

35-P-24-084

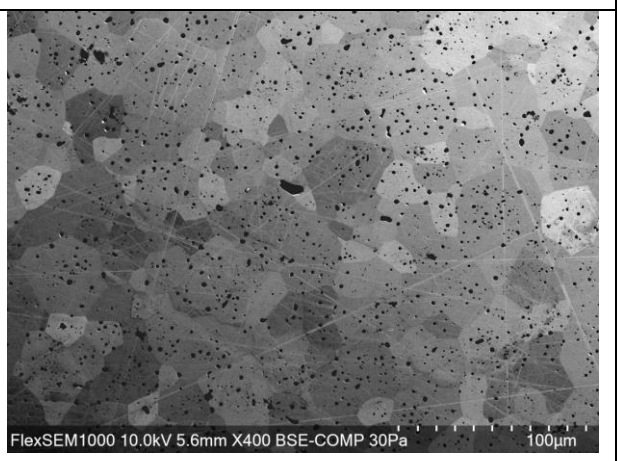

35-P-24-085

Batch 24-013-MF

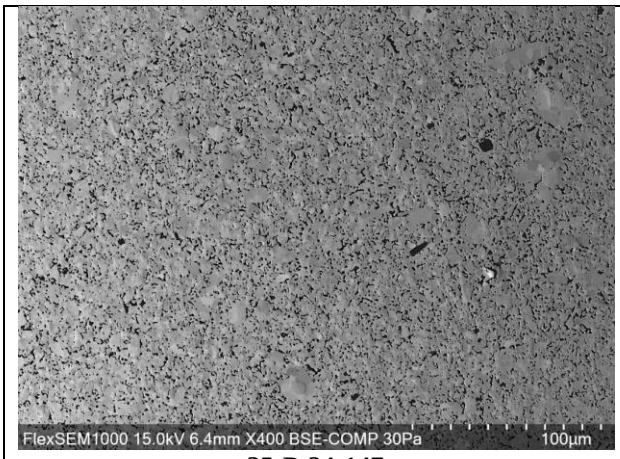

35-P-24-147

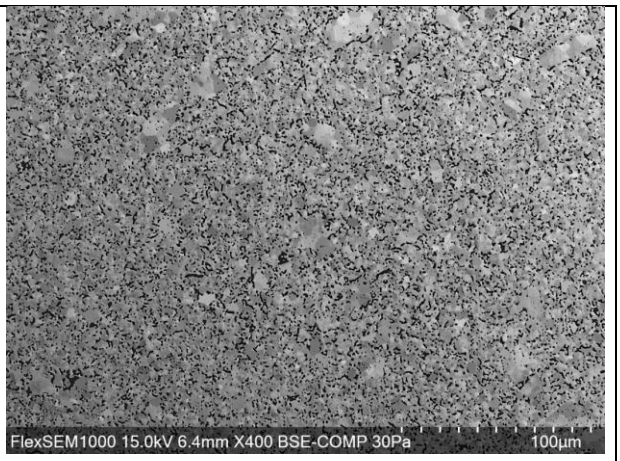

35-P-24-148

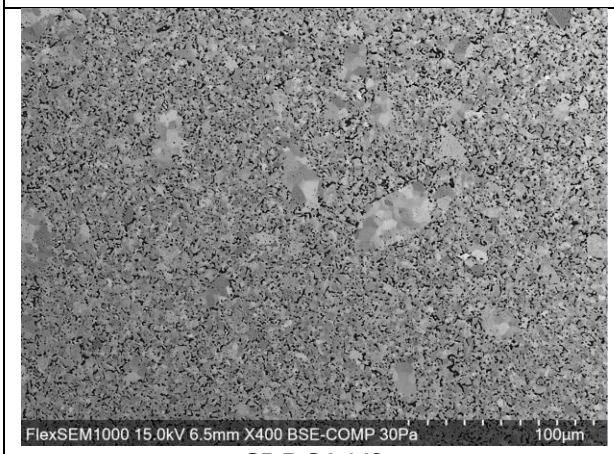

35-P-24-149

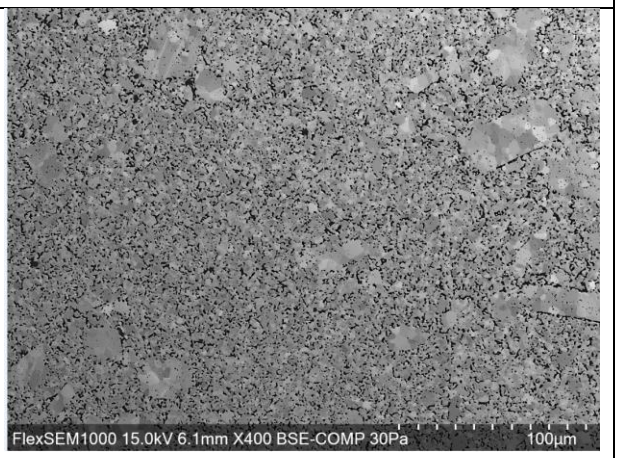

35-P-24-150

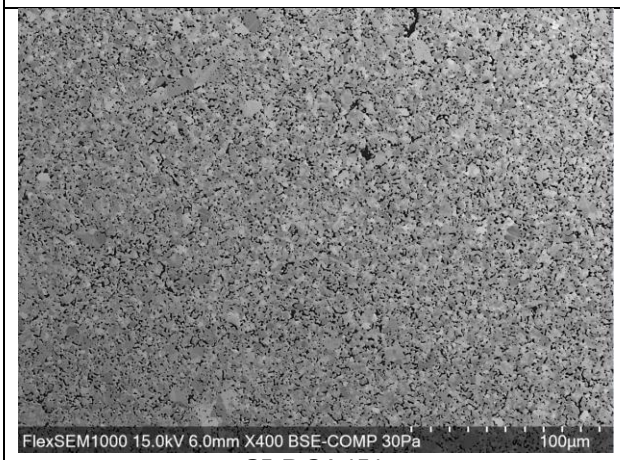

35-P-24-151

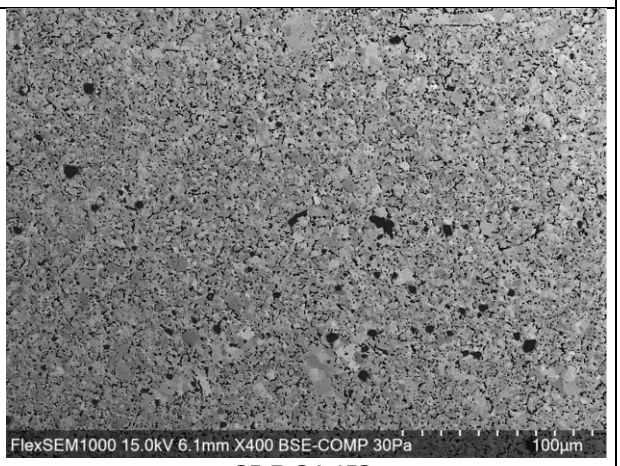

35-P-24-152

Batch 24-014-MF

35-P-24-160

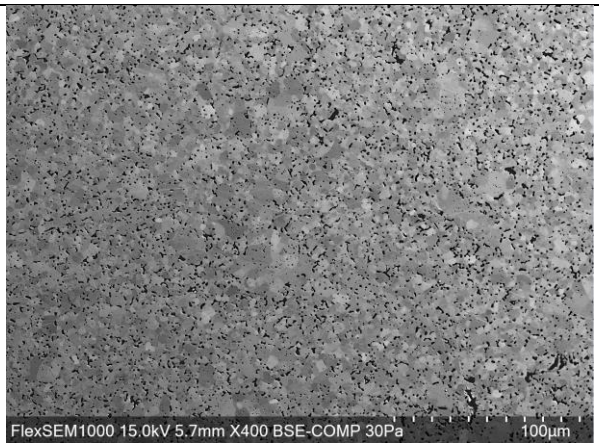

35-P-24-161

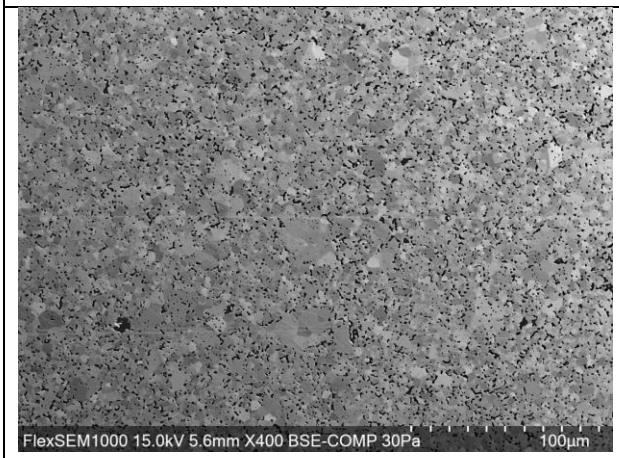

35-P-24-162

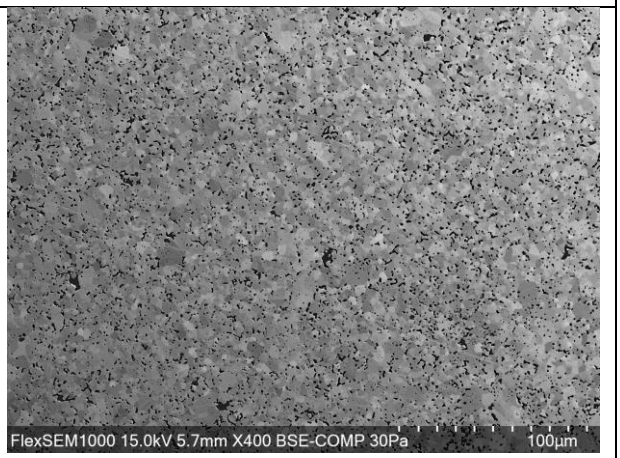

35-P-24-163

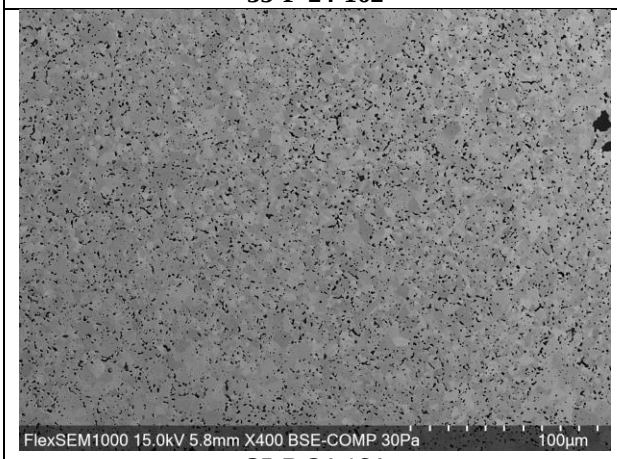

35-P-24-164

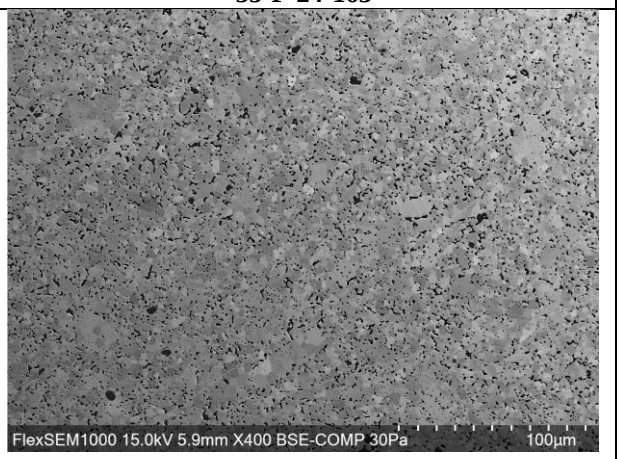

35-P-24-165

Batch 24-015-MF

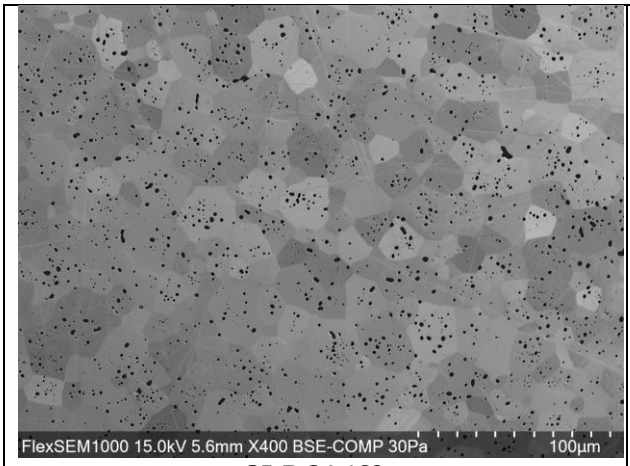

35-P-24-168

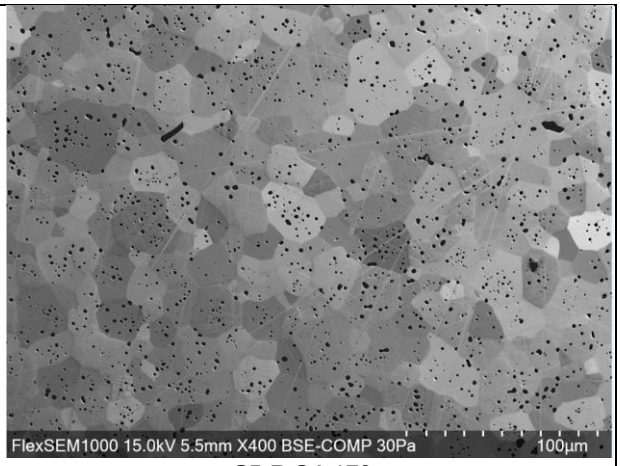

35-P-24-170

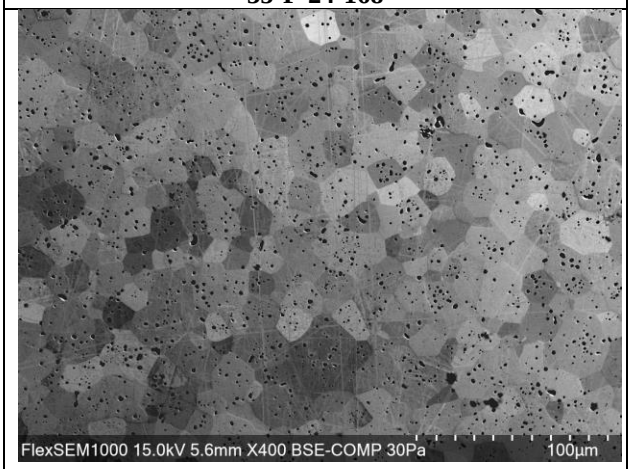

35-P-24-171

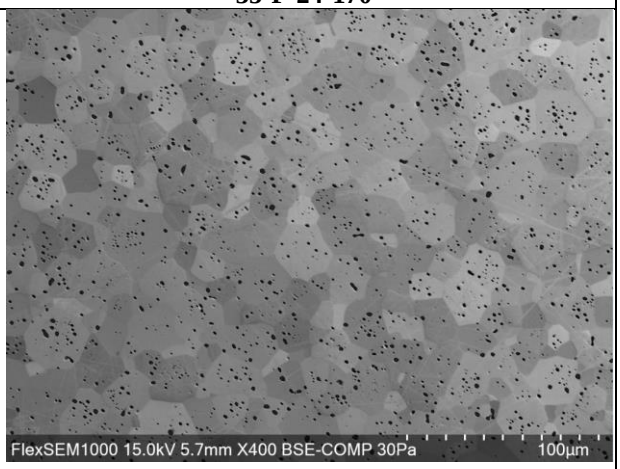

35-P-24-173

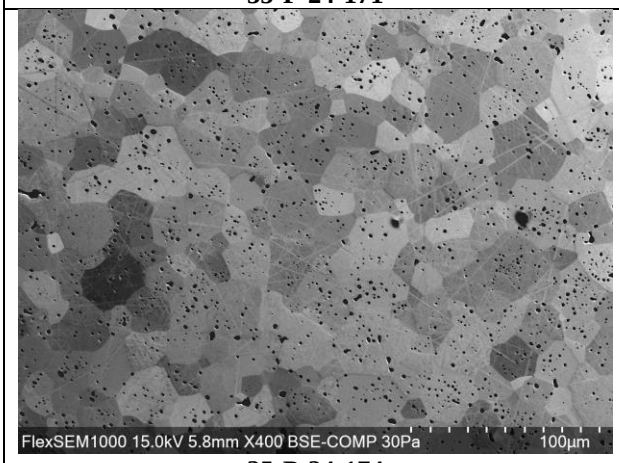

35-P-24-174

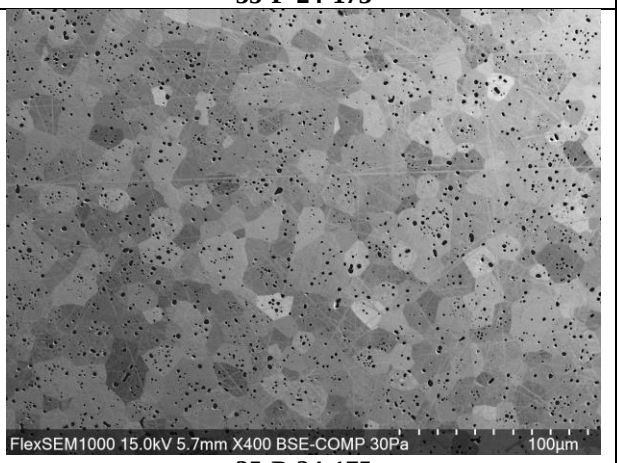

35-P-24-175